

GRADIENT VECTOR FLOW DRIVEN ACTIVE SHAPE FOR IMAGE SEGMENTATION*

Xiaohui Yuan, Balathasan Giritharan, JungHwan Oh

Department of Computer Science and Engineering
University of North Texas
Denton, TX 76203
{xyuan, giri, jhoh}@unt.edu

ABSTRACT

We describe a gradient vector flow driven active shape method for model-based image segmentation. Active shape algorithm retain the shape feature of the interested object, and its performance relies heavily on initialization. Because of a lack of global regulation, the control points tends to be trapped in a local optimum in searching. Our proposed method uses the gradient vector flow of an image to guide the optimization process. The control points of an active shape are steered by the direction and the magnitude of gradient vectors. Our experiments demonstrated great improvement in finding the global optimum and resulting correct segmentation.

1. INTRODUCTION

The active shape model (ASM) [1] has been developed to constrain the image segmentation process for targeted objects. Its advantage over many other methods is that it integrates shape feature into snake evolution. The control points on the searching contour are attracted by local edge gradients and deform to enclose the targeted object. Adjustment of the control points is done via mapping back to the learned shape. The initialization of an ASM-based method is critical because of its local search strategy and lack of global regulation. Poor initialization tends to result in an erroneous outcome.

To address this issue, we have developed a gradient vector flow driven ASM that integrates the gradient vector field as an external force to bring the trapped control points out of local optima. The gradient vector flow is first computed from an enhanced input image, and then trivial edges and noise are eliminated. It is independent from the shape model and captures the gross gradient structure of the image. The updating of the control points in the ASM is regulated by the gradient vectors in terms of direction and step size.

The rest of this paper is organized as follows: In Section 2, we briefly review related work on the ASM method. In Section 3, we describe our method in detail. In Section 4, experimental result is presented with discussions. In Section 5, we summarize our method and conclude this paper.

* THIS WORK IS SUPPORTED BY NSF IIS-0722106.

2. RELATED WORK

The ASM [1] is a parametric deformable shape description in which a statistical abstraction of the global shape variation is constructed from training samples. In ASM-based methods, a point distribution model is computed from examples of the shape. A shape is represented with n points annotated by human experts. These points are organized into a vector form:

$$X = \{x_1, y_1, x_2, y_2, \dots, x_n, y_n\}^T \quad (1)$$

where (x_i, y_i) are the coordinates of the i th annotated point. By performing a principal component analysis (PCA) of the annotated images of the training set, one can build an abstraction that describes the most significant shape variations among the training samples. Such an abstraction is represented as eigen vectors, and an approximation can be approximately reconstructed from these eigen vectors by using the following equation:

$$X \simeq \bar{X} + Pb \quad (2)$$

where \bar{X} denotes the mean shape of the training set, $P = (p_1|p_2|\dots|p_q)$ consists of the q most significant eigen vectors of the covariance matrix, and b is a q dimensional vector that defines the model parameters. By allowing a variation range, this method ensures the gross similarity among shapes.

When ASM is applied to an image, the mean shape is usually the starting point. The control points of the initialization explore the neighborhood following the normal direction to find suitable optimization for the target contour. Figure 1 illustrates an ASM with control points denoted by black dots. Using the target points and the current model, estimates are made for translation (x_t, y_t) , rotation θ , and scaling s . The parameter b is updated based on Equation 2 and the transformation function T :

$$X = T_{x_t, y_t, \theta, s}(X + Pb) \quad (3)$$

This process is iterated until b converges or little change is seen among all control points. However, the ASM uses a local searching method and may fail to locate an acceptable result

if it is initialized too far from the target [1]. An example with poor initialization is shown in Figure 2. Figure 2(a) is the initial contour and (b) is the result after 20 iterations. The model is trapped on the right side of the image.

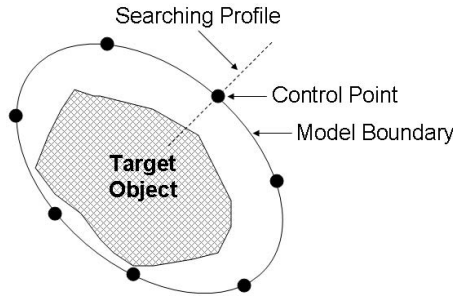


Fig. 1. Control points move along the normal to the model boundary.

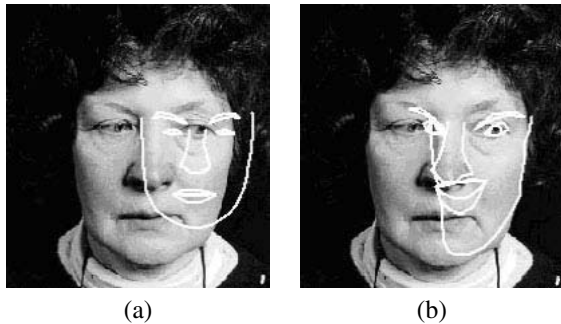


Fig. 2. Segmentation with ASM given a poor starting point [1]. The contour in (a) illustrates the initialization and (b) is the segmentation result.

3. GRADIENT VECTOR FLOW DRIVEN ACTIVE SHAPES

The inadequacy of the ASM is caused by the local searching scheme. The exploration of control points is defined by the normal direction of the model contour. To account for this problem, Ginneken [2] proposed a method using a classifier. Examples of features at the correct location and examples of features at nearby incorrect locations are collected, and a classifier is constructed. This classifier is then used to find the point that is most likely to be true position and least likely to be background. This approach was applied to segment lung fields in chest radiographic images. Our intention of addressing this issue is to aggregate a global external force to lead the control points out of the local optima without an additional data structure.

The gradient vector flow of an image is independent of the evolving active contour and is constructed from the edge map [3]. An edge map $f(x, y)$ is derived from the image

$I(x, y)$. The gradient of an edge map, ∇f , has vectors pointing toward the edges. In the homogeneous regions, the vectors are small; whereas in the vicinity of the edges, the vectors have great magnitudes. The gradient vector flow field is defined to be the vector field $V(x, y) = [u(x, y), v(x, y)]$ that minimizes the energy function:

$$\epsilon = \iint \mu(u_x^2 + u_y^2 + v_x^2 + v_y^2) + |\nabla f|^2 |V - \nabla f|^2 dx dy \quad (4)$$

Figure 3 illustrates a sub-plot of the gradient vector flow field. It is shown that on both sides of an edge, the vectors are pointing toward the edge, which forms a sink, and that an exploring control point can easily find a balanced position. This is a good property when this strong edge is the target. Otherwise, a few control points may be stalled. Stalling can be rectified by remapping using PCA approximation.

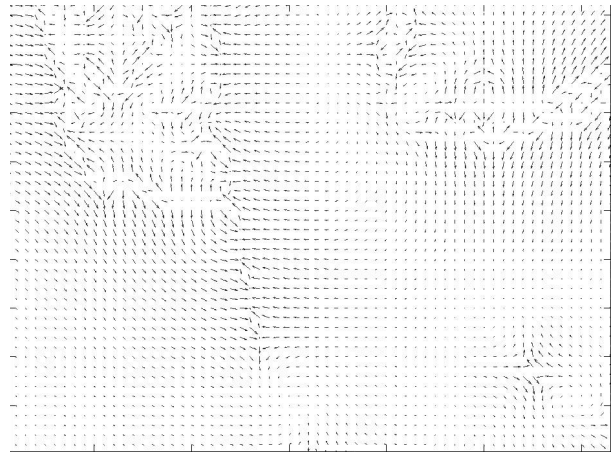


Fig. 3. Sub-plot of the gradient vector flow of a test image.

Using calculus of variations, Gradient Vector Flow (GVF) can be found by solving the following equation:

$$\begin{aligned} \mu \nabla^2 u - (u - f_x)(f_x^2 + f_y^2) &= 0 \\ \mu \nabla^2 v - (v - f_y)(f_x^2 + f_y^2) &= 0 \end{aligned} \quad (5)$$

The numerical implementations of Equation (5) are achieved by treating u and v as functions of time and solving these equations gives

$$\begin{aligned} u_{i,j}^{n+1} &= (1 - b_{i,j} \nabla t) u_{i,j}^n + r(u_{i+1,j}^n + u_{i,j+1}^n \\ &\quad + u_{i-1,j}^n + u_{i,j-1}^n - 4u_{i,j}^n) + c_{i,j}^1 \Delta t \\ v_{i,j}^{n+1} &= (1 - b_{i,j} \nabla t) v_{i,j}^n + r(v_{i+1,j}^n + v_{i,j+1}^n \\ &\quad + v_{i-1,j}^n + v_{i,j-1}^n - 4v_{i,j}^n) + c_{i,j}^2 \Delta t \end{aligned} \quad (6)$$

where

$$\begin{aligned} b(x, y) &= f_x(x, y)^2 + f_y(x, y)^2 \\ c^1 &= b(x, y) f_x(x, y) \\ c^2 &= b(x, y) f_y(x, y) \\ r &= \frac{\mu \Delta t}{\Delta x \Delta y} \end{aligned}$$

To integrate the gradient vector flow field with the ASM, we used the gradient vectors as the searching profile for each control point on the contour of ASM. Let $X, X = \{c_1, c_2, \dots, c_n\}$ and denote the current coordinates of the control points on ASM and $X', X' = \{c'_1, c'_2, \dots, c'_n\}$, denote the coordinates of the control points in the previous iteration, where c is a tuple of $[x \ y]$. Then X can be represented by X' given a step size w :

$$X = X' + wV(X') \quad (7)$$

where $V(X)$ is the gradient vectors at the locations defined by X . Note that for each $V(c_i)$, both the magnitude, $\|wV\|$, and direction, $\arctan(V_y/V_x)$, differ. This difference ensures a search along the direction of the gradient vector field. The gradient vectors are larger near strong edges and slowly vary near weak edges. When an initialization is placed far away from the target, the gradient vectors guarantee a faster convergence toward the desired location.

Another issue to be addressed is leakage; that is, the segmenting contour continues expanding outside the object of interest. This problem is common with the contour-based segmentation method and usually depends on the searching function and stopping criteria. The searching footprint in the ASM is fixed. Given a very distinctive boundary, an ASM can land all control points at the right locations. However, a faint edge is sometimes the preferred site. Examples are shown in Figure 4(a) and (b). The chin and the neck have a very weak boundary. Hence, the gradient vectors are small but can lead the control point out of the region. In addition, when gradient vector magnitude becomes a factor in search profile, a larger footprint usually occurs at a later iteration, which could lead to an in-converged outcome. If the initialization is placed in a uniform region, because of small gradient vectors, it takes much longer for the model to converge. Here, we assign an annealing factor to gradually reduce the step size along iteration. This annealing factor, denoted by k , is inversely proportional to the time. Therefore, the searching equation becomes

$$X = X' + wkV(X') \simeq X' + w\frac{p}{t^q}V(X') \quad (8)$$

where p and q are constants of the annealing factor. They can be specified depending on the images. In general, both shall be greater than, or equal to, one.

By giving appropriate scaling, translation, and rotation parameters, the user initializes a shape model based on the mean shape found by performing PCA. The exploration of control points continues until it converges. The convergence function F is defined as minimizing the difference of control points between two consecutive iterations:

$$F(X, X') = \sum_{i=1}^n \|X_i - X'_i\|_2 \quad (9)$$

The Euclidean difference of all control points from their previous and current locations is computed. A threshold is specified to halt the searching process.

At each iteration, after the subsequent locations for all control points are found, the translation (x_t, y_t) , scaling s , and rotation θ of the model are calculated. The model parameter b is updated using Equation 2, so that the contour X is cast to a new set of coordinates that is constrained by the learned shape components P using Equation 3.

4. RESULTS AND DISCUSSION

4.1. Data Preparation and Experimental Setup

We have implemented our method in MATLAB. In our experiments, annotated images of human faces were used for training and testing. The model for the face outline was learned from the XM2VTS frontal data set [4]. This training set contains 2360 mug shots of 295 individuals, and the learned model was then used for segmentation of face images obtained from the BioID database [5]. Before applying our method to the test images, we used a 3 by 3 Gaussian filter to remove possible noise. All the images were converted, as necessary, into 8-bit grayscale. Canny edge detector was used to construct the edge map for the computation of the gradient vector field.

4.2. Experimental Results

In our experiments, random initializations were used for all segmentation tests. We used the center of gravity of the contour as the reference for both the initialization and the evaluation. According to the distance between the center of reference contour and the center of the initialization, we categorized the initialization into three intervals: less than 5 pixels, 6 to 15 pixels, and 16 to 25 pixels. With the same initialization, experiments were done using conventional ASM and our method. Table 1 presents the average and standard deviation of both methods using 10 repetitions on 5 sets of images.

In each interval, we calculated the overall mean and standard deviation. As shown in Table 1, when the initialization is close to the target, both methods yielded similar performance. With increased deviation from the target, our method resulted in better segmentation with a smaller mean value and a smaller standard deviation.

Figure 4 illustrates three screen captures of the experiments using our method. The first row shows the initialization contour, ves. The dots on the curve illustrate the control points of the contour model. Compared to Figure 2, given the similar initializations, our method successfully segmented the targets.

5. CONCLUSIONS

In this article, we present a segmentation method using a gradient vector flow driven active shape model. Our method extends ASM to integrate the gradient information to avoid local optima in the searching process. In contrast to the ex-

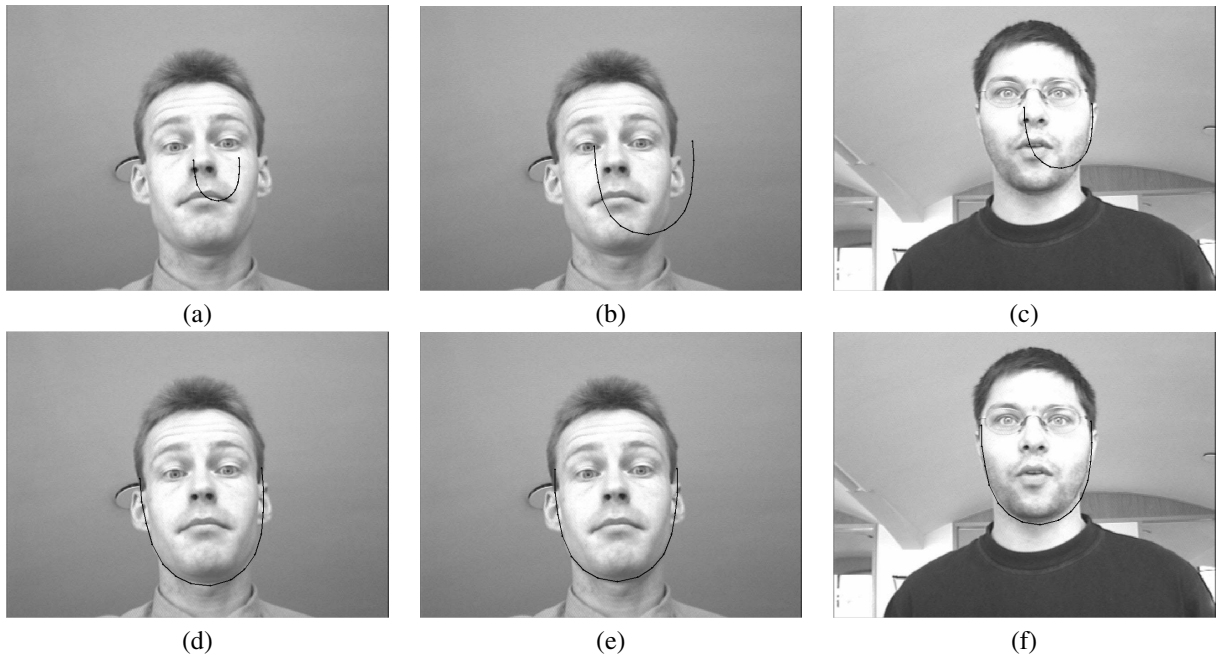


Fig. 4. Sample results using our method. (a)–(c) are the initialization contours. (d)–(f) are the segmentation results.

Table 1. Segmentation results using random initialization with respect to the center of the contour.

Number of Pixels	Test Cases	ASM		G-ASM	
		mean	std	mean	std
<5	1	3	1.2	2.9	0.8
	2	3.8	1.6	3.0	1.4
	3	3.3	1.3	3.2	1.2
	4	3.9	1.0	3.8	1.8
	5	3.6	1.0	3.7	0.9
	Overall	3.5	1.3	3.3	1.3
6–15	1	5.4	1.3	3.5	1.6
	2	4.8	2.0	3.8	1.6
	3	4.6	2.0	3.4	1.2
	4	4.8	1.6	2.9	1.7
	5	4.1	2.0	3.8	1.6
	Overall	4.7	1.8	3.5	1.5
16–25	1	4.9	2.1	3.3	1.0
	2	5.2	2.9	3.9	1.6
	3	6.1	2.1	3.4	1.5
	4	4.9	2.5	2.7	1.5
	5	7.3	2.5	3.8	1.6
	Overall	5.7	2.5	3.5	1.4

ploratory profile of control points of a conventional ASM, our method uses gradient to guide searching for the next best fit. Additionally, to avoid leaking, we used an annealing factor to reduce the step size gradually so that the segmentation process converges successfully. A comparison study was conducted, and experimental results demonstrated that our method improves robustness and accuracy of the segmenta-

tion. Although our evaluation was based on face images, this method can be easily extended to segment other methods. By using texture and color information, one can also achieve edgeless segmentation [6].

6. REFERENCES

- [1] T. F. Cootes and C. J. Taylor, “Combining point distribution models with shape models based on finite-element analysis,” *Image and Vision Computing*, vol. 13, no. 5, pp. 403 – 409, 1995.
- [2] B. van Ginneken, *Computer-Aided Diagnosis in Chest Radiography*, Ph.D. thesis, University Medical Centre Utrecht, Netherlands, 2001.
- [3] C. Xu and J. L. Prince, “Snakes, shapes, and gradient vector flow,” *IEEE Transactions on Image Processing*, vol. 7, no. 3, pp. 359 – 369, 1998.
- [4] “<http://www.ee.surrey.ac.uk/research/vssp/xm2vtsdb/>,” The Extended M2VTS Database.
- [5] “<http://www.bioid.com/downloads/facedb/index.php>,” Human Scan, BioID.
- [6] C. Sagiv, N. A. Sochen, and Y. Y. Zeevi, “Integrated active contours for texture segmentation,” *IEEE Transactions on Image Processing*, vol. 15, no. 6, pp. 1633 – 1646, 2006.